Talanta xx (xxxx) xxxx–xxxx

Contents lists available at ScienceDirect

Talanta

journal homepage: www.elsevier.com/locate/talanta

A novel aptameric biosensor based on the self-assembled DNA–WS_2 nanosheet architecture

Aixue Li[a,1], Jian Zhang[b,1], Jichuan Qiu[c], Zhenhuan Zhao[c], Cheng Wang[a], Chunjiang Zhao[a,*], Hong Liu[c,*]

[a] Beijing Research Center for Information Technology in Agriculture, Beijing Academy of Agriculture and Forestry Sciences, Beijing 100097, China
[b] Université de Lyon, ECL, INSA-Lyon, UCBL, CPE, CNRS, INL, UMR 5270, 36 Avenue Guy de Collongue, 69134 Ecully Cedex, France
[c] State Key Laboratory of Crystal Materials, Shandong University, Jinan 250100, China

ARTICLE INFO

Keywords:
Aptamer
Biosensor
Tungsten disulfide
ATP
Hg^+

ABSTRACT

It has been reported that tungsten disulfide (WS_2) can bind single-stranded DNA (ssDNA) with high affinity while it has less affinity toward double stranded DNA (dsDNA). In this work, for the first time, the high affinity between WS_2 and ssDNA was used to construct stable sensing interface for ATP detection. A DNA sequence with –SH at one end was first immobilized on Au electrode. WS_2 nanosheets were immobilized on the SH-DNA/Au electrode surface due to the strong affinity between WS_2 and ssDNA. Then the WS_2 nanosheets were used to immobilize ATP binding aptamer (ABA) through the high affinity between WS_2 and ssDNA, too. When ATP reacts with the ABA aptamer, duplex will be formed and dissociated from the WS_2 nanosheets. On the basis of this, an electrochemical aptasensor for ATP was fabricated. This ATP sensor showed high sensitivity, selectivity and stability due to the unique WS_2-ssDNA interactions and the specific aptamer–target recognition. Furthermore, this strategy was generalized to detect Hg^{2+} using a mercury-specific aptamer (MSO). This strategy can be expected to offer a promising approach for designing high-performance electrochemical aptasensors for a spectrum of targets.

1. Introduction

Aptamers are short, single-stranded, functional DNA or RNA structures, generated from random-sequence nucleic acid libraries and can be chemically synthesized [1–3]. They possesses a series of excellent properties, such as high specificity in molecular recognition, broad range of targets from small inorganic and organic substances to proteins and cells, good stability, lack of immunogenicity, low cost, and controllable in modification [4–7], etc. Now, aptamers have been extensively utilized to construct various biosensors [8–10].

Among varied analytical methods, electrochemical methods is attractive because of its operation simplicity, low expense of instruments, suitability for real-time detection and lower sensitivity to matrix effects [11]. A variety of electrochemical biosensors have been developed for biological and environmental analysis [12–15]. In the electrochemical sensors, biological sensing elements (e.g., enzymes or antibodies) are immobilized/integrated at the electrochemical interface. Upon target binding, the electrochemical signal is changed, which is directly related to the concentration of target. Therefore, engineering the electrochemical sensing interface is important for improving the sensitivity and stability of electrochemical biosensors. In the electrochemical field, the aptamer-target recognition events can be easily converted into detectable electrochemical signals. Moreover, the coupling of aptamers with nanomaterials will lead to the development of novel biosensors with more promising performances [16–18].

In recent years, layered two-dimensional (2D) transition metal dichalcogenides (TMDCs) with single or few atomic layers, have received much attention owing to their special structures with high specific surface area and unusual electronic properties [19–25]. Tungsten disulfide (WS_2) nanosheets are archetypical examples of inorganic analogues of graphene [26,27]. Layered WS_2 consists S–W–S sandwiches in a trigonal prismatic coordination [28,29]. Compared with graphene, WS_2 nanosheets can be synthesized on a large scale and dispersed in aqueous solutions directly, indicating that WS_2 nanosheets have great potential as a novel nanomaterial for biomedical applications [30–34]. However, the exploration of WS_2 nanosheets as a bioanalytical platform is still at an early stage.

It has been reported that graphene oxide (GO) can bind and quench

* Corresponding authors.
E-mail addresses: zhaocj@nercita.org.cn (C. Zhao), hongliu@sdu.edu.cn (H. Liu).
[1] These authors contributed equally to this work.

http://dx.doi.org/10.1016/j.talanta.2016.10.088
Received 18 July 2016; Received in revised form 20 October 2016; Accepted 23 October 2016
Available online xxxx
0039-9140/

dye-labelled single stranded DNA (ssDNA) probes, while it has less affinity towards double-stranded DNA (dsDNA) or secondary and tertiary structured ssDNA [35–38]. More recently, MoS_2 and WS_2 nanosheet have also been reported to possess the capability for discriminating single stranded DNA (ssDNA) and double stranded DNA (dsDNA) [39–42], which may catalyze the applications of transition metal dichalcogenides nanosheets in biosensing field.

In this work, for the first time, the high affinity between WS_2 and ssDNA was utilized to construct stable sensing interface for ATP detection. As shown in the scheme, a DNA sequence with –SH group at one end was first immobilized on Au electrode via the Au–S chemistry. WS_2 nanosheets were immobilized on the DNA layer due to the strong affinity of the WS_2/ssDNA interaction. Then the WS_2 nanosheets were used to immobilize adenosine triphosphate binding aptamer (ABA) through the unique WS_2/ssDNA interaction, too. The step by step modification of the DNA, WS_2 nanosheets and aptamer on the electrode will lead to an increase in the charge transfer resistance (R_{ct}). However, the binding reaction between aptamer and its target adenosine triphosphate (ATP) would form duplex which have weak affinity with the WS_2 nanosheets; as a result, R_{ct} will be decreased. On the basis of this, we fabricated an electrochemical aptasensor for the detection of ATP. The sensor showed high sensitivity and specificity for its targets due to the excellent properties of aptamer. During the whole fabrication, only the Au–S chemistry and the strong WS_2/ssDNA interaction were used, so this ATP sensor also showed high stability. Moreover, it is fairly easy to generalize this approach to detect Hg^{2+} using a mercury-specific, thymine (T)-rich oligonucleotide aptamer (MSO) (Scheme 1).

2. Experimental section

2.1. Materials

All DNA sequences were synthesized and purified by Shanghai Sangon Biotechnology Co. Ltd (Shanghai, China). The oligonucleotides have the following sequences:

SH-DNA (This sequence is non-complementary for ABA and MSO): 5′ SH-C6- GCTCTGCGTTATCAGACTGA -3′

ABA: 5′-ACCTGGGGGAGTATTGCGGAGGAAGGT-3′,

MSO: 5′-ATTCTTTCTTCCCCCCGGTTGTTTGTTT-3′,

DNA stock were prepared with Tris-HCl buffer (25 mM Tris-HCl, 150 mM NaCl, pH=8.0). ATP, cytidine triphosphate (CTP), thymidine triphosphate (TTP), and guanosine (GTP) were purchased from Sigma-aldrich and prepared in the Tris-HCl buffer. The metal salts ($Hg(Ac)_2$, $Pb(Ac)_2$, $CdCl_2$, $CaCl_2$, $FeCl_3$, $Cu(Ac)_2$, $Mg(Ac)_2$, $ZnSO_4$, $AgNO_3$) were provided by Guoyao Co., Ltd. (Beijing, China) and used directly. 2-Mercaptoethanol (MCE), WCl_6 and thioacetamide (C_2H_5NS) was bought from Sigma-aldrich. The other reagents were of analytical reagent grades, which also were bought from Guoyao Co., Ltd. (Beijing, China). The human serum had been got from the 307th Hospital of Chinese People's Liberation Army. Doubly distilled water (DDW) was used throughout the experiments.

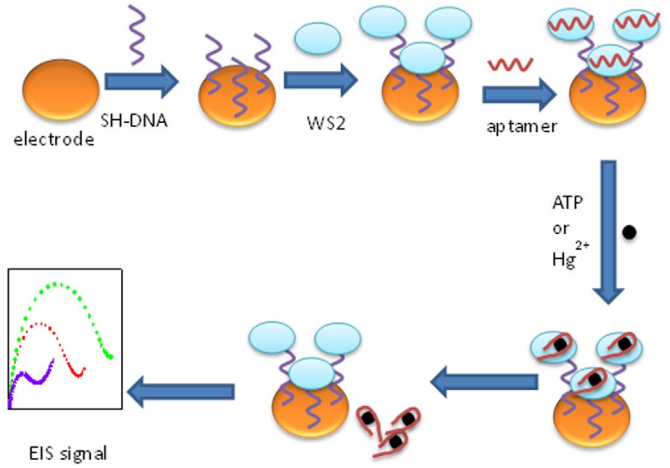

Scheme 1. Schematic illustration of the electrochemical sensing strategy for the detection of ATP or Hg^{+}.

2.2. Preparation of few layered WS_2 sheets

WS_2 sheets were synthesized by a one-step hydrothermal reaction according to the previous report [43]. Briefly, 3 mM WCl_6 and 15 mM C_2H_5NS were dissolved in 40 mL DDW water and stirred for 1 h using a magnetic stirrer at room temperature. The solution was transferred to a 50 mL autoclave, heated to 250 °C and kept for 30 h. After cooling naturally, the product was filtered and washed. Then the product was dried in a vacuum at 50 °C for 8 h.

2.3. Characterizations

The WS_2 nanosheets were characterized with X-ray diffraction on a Bruker D8 Advance powder X-ray diffractomer (D8-advance, BrukerAXS, Germany) with Cu-Kα radiation (λ=0.15406 nm), scanning electron microscopy (HITACHI S-8020 microscopy, Japan) and Raman spectrometer (HORIBA/LabRAM HR Evolution, France) with a laser excitation wavelength of 532 nm and laser power of 1 mW/cm^2. For characterization of the fabrication process of the electrode, surface plasmon resonance (SPR), Atomic force microscopy (AFM), and X-ray photoelectron spectroscopic (XPS) were used. For the SPR, AFM and XPS experiments, the samples were prepared on cleaned Au substrate, and the modification process was the same as that on the electrode surface. The angle-resolved SPR measurements were performed using a Autolab SPR instrument (Eco Chemie BV, The Netherlands). This instrument worked with a laser diode fixed at a wavelength of 670 nm, a vibrating mirror was used to modulate the angle of incidence of the p-polarized light beam on the SPR substrate. AFM was performed on a SPI3800N microscope instrument (Seiko Instruments, Inc., Japan) in a tapping-mode at room temperature. XPS were performed on a Thermo Fisher Scientific ESCALAB 250Xi spectrometer (Thermo Fisher Scientific, Inc, Waltham, MA, USA) with Al Kα excitation, and C1s (284.5 eV) was used to calibrate the peak positions of the elements.

2.4. Electrode preparation and fabrication of the sensing interface

Au electrode (1.6 mm in diameter, Shanghai Chen Hua Instrument Co., Ltd, China) was polished carefully with 1, 0.3, and 0.05 μm alumina powder sequentially and then washed ultrasonically in water and ethanol for a few minutes, followed by electrochemically cleaning in 1 M H_2SO_4 by cyclic potential scanning between –0.2 and 1.55 V until a standard cyclic voltammogram was obtained. Subsequently, the Au electrode was rinsed with copious amounts of DDW and absolute ethanol in turn.

Au electrode was first immersed in 15 μM SH-DNA solution for 20 h to assemble the DNA monolayer through the Au–S bond between DNA and Au substrate, followed by rinsing with buffer. The electrode was dried in a nitrogen stream, after which the interface was incubated in 10 μM MCE and kept for 4 h. The modified Au electrode was put into 0.1 mg/mL WS_2 solution for about 24 h to immobilize WS_2 nanosheet, followed by rinsing with copious water. The WS_2 nanosheet modified electrode was incubated in 50 μM ABA solution for 24 h to immobilize aptamer. The electrode was rinsed with Tris-HCl buffer and dried with nitrogen, and the aptamer modified electrode was obtained.

2.5. Electrochemical detection of ATP

The concentration of SH-DNA and ABA to be immobilized onto the electrode surface was optimized. The optimized concentration for SH-

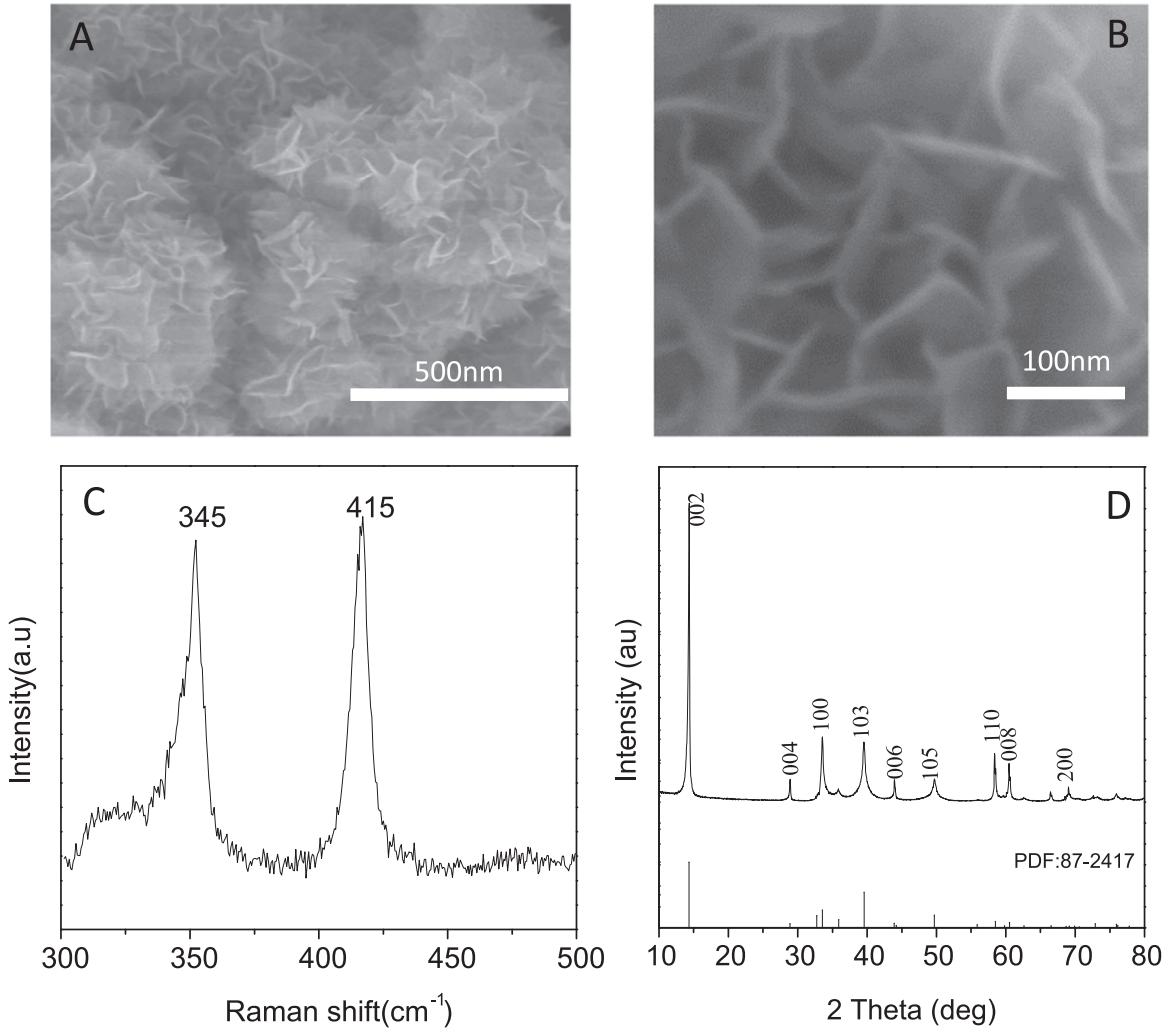

Fig. 1. low- (A) and high-magnification (B) FESEM images of WS_2 nanosheets. (C) Raman spectra and (D) XRD pattern of WS_2 nanosheets.

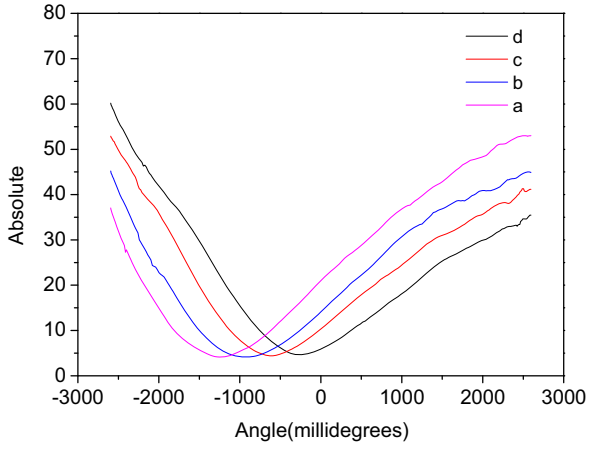

Fig. 2. Angle-resolved SPR curves for the modification of the Au substrate. a, Au substrate; b, SH-DNA layer; c, WS2; d, ABA aptamer.

DNA and ABA was 10 μM and 50 μM, respectively. Therefore, 10 μM SH-DNA and 50 μM ABA was used to fabricate the ATP sensing interface. The new as-prepared ABA modified electrode was immersed in series concentrations of ATP and reacted for 1 h, followed by washing with buffer. The detection process for TTP, GTP and CTP were the same as those used for ATP detection.

For investigating the stability of the constructed ATP sensor, a control sensor was also prepared. Au electrode was first immersed in 10 μM MCE solution for 4 h, and then 5 μL WS_2 solution (0.1 mg/mL) was dropped on the MCE surface and allowed to dry at room temperature. 5 μL aptamer for ATP (ABA) at the optimized concentration (50 μM) was dropped onto the electrode surface and dried at room temperature. The electrode was washed gently with Tris-HCl buffer to remove excess, nonadsorbed material.

A conventional three-electrode system was used for the electrochemical measurements. The modified Au electrode was used as working electrode, Ag/AgCl (saturated KCl) electrode (Shanghai Chen Hua Instrument Co., Ltd, China) was used as reference electrode, and a Pt plate (Shanghai Chen Hua Instrument Co., Ltd, China) was used as counter electrode. A Gamry reference 3000 (Gamry Instruments, America) were used for the electrochemical measurements. The electrochemical measurements were performed in 0.01 M phosphate buffer solution (pH 7.4) containing 0.1 M KCl using 5 mM $K_3[Fe(CN)_6]/K_4[Fe(CN)_6]$ (1:1) mixture as a redox probe. The impedance spectra were performed in the frequency range from 100 mHz to 100 kHz versus Ag/AgCl (saturated KCl) with a voltage amplitude of 5 mV.

2.6. Electrochemical detection of Hg^+ based on MSO and WS_2

The fabrication process of the Au electrode for the Hg^+ sensor was the same as that described for ATP except using the mercury-specific aptamer (MSO) instead of ABA. The concentration of SH-DNA and

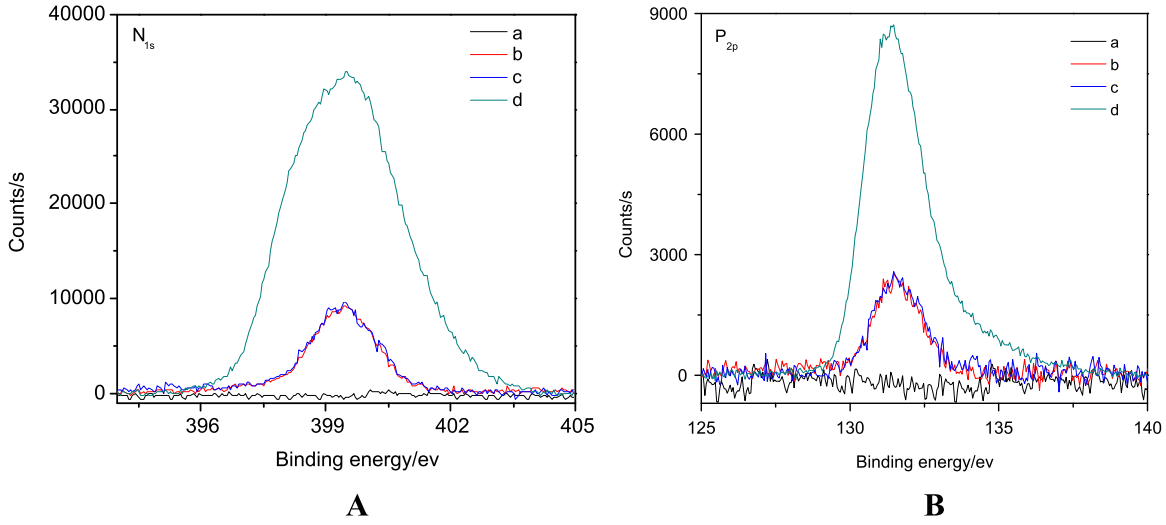

Fig. 3. XPS spectra of (A) N_{1s} and (B) P_{2p} for the modification of the Au substrate. a, Au substrate; b, SH-DNA layer; c, WS_2; d, ABA aptamer.

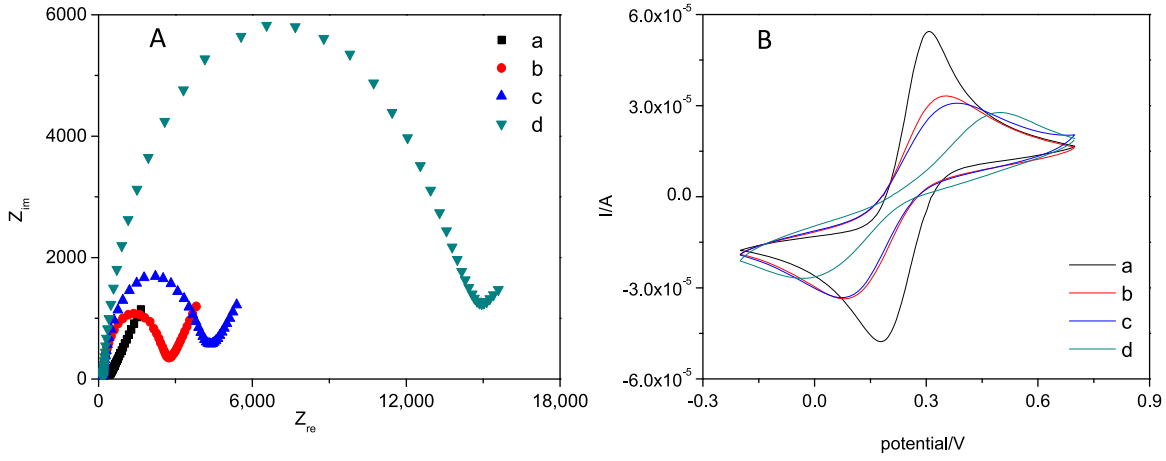

Fig. 4. Complex impedance plot (A) and CV plot (B) for the layer by layer modification process of the Au electrode in the presence of 5 mM $[Fe(CN)_6]^{3-/4-}$ in 0.01 M PBS (pH 7.4, containing 0.1 M KCl). a, Au electrode; b, SH-DNA/Au electrode; c, WS_2/SH-DNA/Au electrode; d, ABA/WS_2/ SH-DNA/Au substrate.

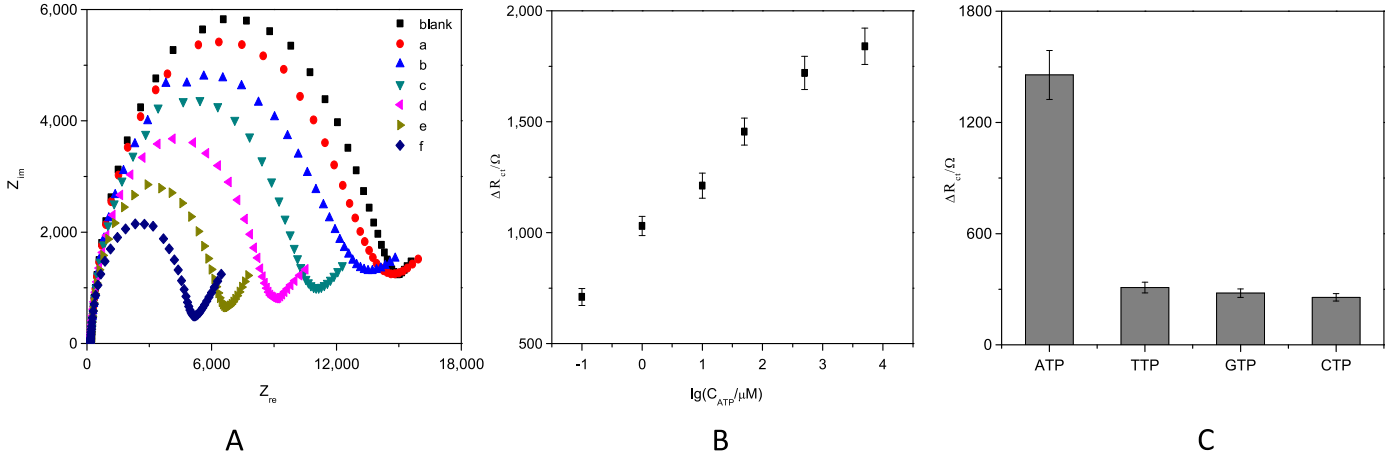

Fig. 5. (A) EIS response for the detection of different concentrations of ATP. a–f: 0.1 μM, 1 μM, 10 μM, 50 μM, 0.5 mM, 5 mM (B) The relationship between ΔR_{ct} and the logarithm of the concentration of ATP. (C) Selectivity for the detection of ATP. ATP and other tested molecules were all used at 50 μM.

MSO for the fabrication was also 10 μm and 50 μm, respectively. For the detection of Hg^+, the MSO modified Au electrode was immersed in different concentrations of Hg^+ and reacted for 1 h, followed by washing. The detection process for other metal ions was the same as those used for Hg^+ detection.

3. Result and discussion

3.1. Characterization of WS_2

WS_2 nanosheets prepared according to one-step hydrothermal reaction were characterized by field-emission scanning electron micro-

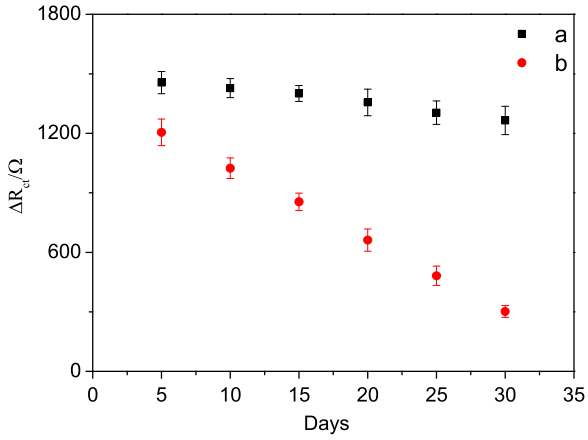

Fig. 6. Stability of the constructed ATP sensor (a) based on the interaction of WS_2 and DNA and a control sensor (b) based on the dropping method for a period of 30 days.

scopy (FE-SEM), Raman spectra, and X-ray diffraction (XRD) (Fig. 1). SEM images reveal that the thickness of WS_2 sheets is ~5–10 nm (Fig. 1a and b). Many WS_2 sheets stacked together, just like a flower or a ball. Raman spectroscopy reveals the characteristic peaks of WS_2 in the 200–500 cm^{-1} range (Fig. 1c), which is agreed with the previous report [44]. XRD analysis of the WS_2 sheets shows high crystalline hexagonal structure (Powder Diffraction File (PDF) No. 87-2417) without any other impurities. The XRD result shows the direction of sheet growth is along the (002) direction (Fig. 1d).

3.2. Modification process for the electrode

SPR spectroscopy is a powerful surface-sensitive technique for detecting analytes adsorbed on a metal surface. In this experiment, it was used to characterize the fabrication procedure of SH-DNA, WS_2, aptamer on a cleaned gold substrate. Fig. 2 showed the angle-resolved SPR curves. In comparison with the blank gold surface (curve a), the SPR angle right-shifted by about 325.1 ± 17 millidegree after immobilizing the SH-DNA layer (curve b). When the WS_2 layer was deposited on the gold substrate (curve c), a right-shift in the SPR angle by about 311.2 ± 15 millidegree was observed. The immobilization of the aptamers (curve d) also resulted in a large SPR angle shift toward higher angles as expected (320.8 ± 18 millidegree). The SPR results confirmed the successful modification of the gold substrate.

AFM technique was also performed to fabricate the self-assembled process of the biosensor construction. AFM image of the bare gold shows uniformly distributed granular nanoporous surface morphology (Fig. S1A). After the assembling of SH-DNA probe (Fig. S1B), the surface of bare Au changes into a well-arranged regular surface morphology indicating the immobilization of SH-DNA probe onto Au surface. After the assembling of WS_2 nanosheets, the WS_2 nanosheets is moss-like on the SH-DNA layer rather than a homogeneous monolayer (Fig. S1C). Similar result has been observed for graphene sheet absorbing on self-assembled monolayer of n-octadecyl mercaptan (C18H37SH) [45]. When the aptamers were further assembled on the WS_2 nanosheets, the mosses become larger (Fig. S1D), indicating the assembling of aptamers on the WS_2 nanosheets. The big-size mosses lead to a very rough electrode surface and large area, which can be used as sensing interface for detecting ATP or Hg^{2+}.

X-ray photoelectron spectroscopic (XPS) measurement can also be used to characterize the assembly of DNA on ITO or Au substrate [46], because there are nitrogen and phosphorus elements in the DNA strands. In this work, it was used to confirm the assembly of SH-DNA and Aptamer on Au substrate. As shown in Fig. 3A, compared with the bare Au substrate (curve a), a small peak of N_{1s} (399.5 eV) can be detected for the SH-DNA/Au sample, suggesting the SH-DNA has been assembled on the Au substrate (curve b). When WS_2 layer was immobilized on the SH-DNA/Au sample, as there is not nitrogen element in WS_2, the XPS spectrum was nearly the same as that of SH-DNA/Au sample (curve c). While after the immobilization of aptamer on the WS_2/SH-DNA/Au substrate, the peak of N_{1s} increases sharply, indicating that aptamer has been assembled on the WS_2/SH-DNA/Au substrate (curve d). Correspondingly, the trend in peak intensity for the P_{2p} (131.4 eV) was consistent with the expected increase in phosphorus content that accompanied the surface modification steps (Fig. 3B, a–d). The XPS results also confirmed the successful modification of the electrode.

EIS and cyclic voltammetry (CV) methods were also used to characterize the layer by layer modification of the electrode in the presence of $[Fe(CN)_6]^{3-/4-}$ (Fig. 4). The concentration of SH-DNA and ABA was optimized (Fig. S2 and S3, Supporting information). The circuit (Fig. S4, Supporting information) was used to fit the EIS data. Compared with the bare Au electrode (Fig. 4A, curve a), the formation of SH-DNA layer (Fig. 4A, curve b) on the Au electrode lead to a large charge transfer resistance (R_{ct}), because the negative charges of the assembled ssDNA repel the negatively charged redox probes. The steric hindrance introduced with the formation of the ssDNA layer on the electrode surface also contribute to the large R_{ct} [47]. When the WS_2 layer was immobilized on the DNA modified-electrode, a further increase in the R_{ct} value can be observed (Fig. 4A, curve c). When the ABA aptamer was immobilized on the WS_2/SH-DNA/Au electrode, the R_{ct} value increase greatly (Fig. 4A, curve d). CV responses for the modification process were also investigated (Fig. 4B). The modification

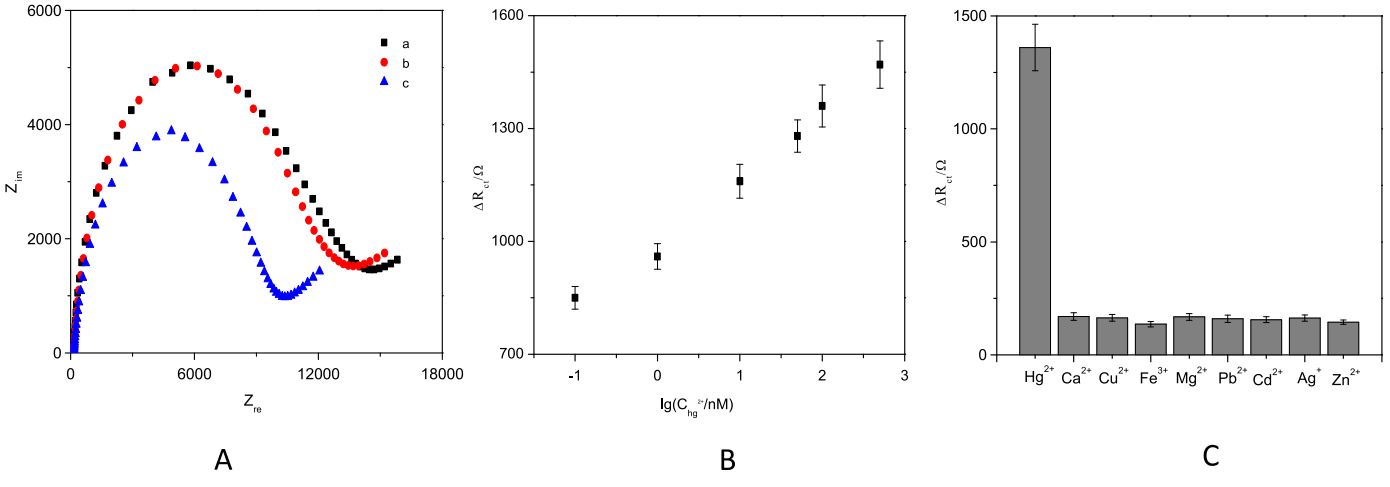

Fig. 7. (A) EIS response for the MSO/WS_2/SH-DNA/Au electrode before (a) and after incubated in blank buffer (b) and reacted with 100 nM Hg^{+}(c). (B) The relationship between ΔR_{ct} and the logarithm of the concentration of Hg^{+}. (C) Selectivity for the detection of Hg^{+}. Hg^{+} and other tested molecules were all used at 100 nM.

of the SH-DNA layer on the electrode surface lead to a decrease of peak current and an increase in peak-to-peak separation between the anodic and cathodic waves of the redox probe. When the WS_2 layer and the aptamer were further immobilized on the SH-DNA modified-electrode in turn, a further decrease of peak current and a large increase in peak-to-peak separation are observed. This illustrates that the layer-by-layer modification of the electrode blocks the interfacial electron-transfer between the redox probe and the surface considerably. The CV result is consistent with that of the EIS measurement.

3.3. Electrochemical detection of ATP

When the modified electrode was incubated in blank buffer for 1 h, the R_{ct} value for the electrode is nearly unchanged, indicating that the sensing interface is very stable. In the presence of ATP, duplex between aptamer and ATP will be formed and dissociated from the WS_2 surface because it has weak affinity with the WS_2 nanosheets; as a result, R_{ct} will be decreased. Fig. 5A shows the EIS response of the modified electrode reacted with series of concentrations of ATP. The R_{ct} gradually decrease with the increased concentrations of ATP. The variation of R_{ct} value (ΔR_{ct}) before and after hybridization with one concentration of ATP (for example, the ΔRct of the 5 mM ATP is variation of R_{ct} value of the remained ABA on the same electrode before and after hybridization with the 5 mM ATP.), has a linear relationship with the logarithmic value of the concentrations of ATP (Fig. 5B), and ATP can be quantified over a concentration range from 0.1 μM to 5 mM (R^2=0.993). The detection limit is estimated to be 1.5 nM according to the 3σ rule, which is more sensitive than the most electrochemical aptasensors that existed for ATP detection [48,49].

The capability in discriminating different nucleotide is crucial for ATP detection. The selectivity of the ATP sensor was investigated using the four kinds of nucleotides (ATP, CTP, TTP, and GTP). As shown in Fig. 5C, a pronounced increase in the ΔR_{ct} value corresponding to the binding with 50 μM ATP is observed, while there is no remarkable ΔR_{ct} shift for CTP, TTP, and GTP. This result suggests that the WS_2-based ATP aptasensor has high selectivity, which may be due to the high specificity of ABA aptamer.

During the whole fabrication process, only the Au–S chemistry and the strong WS_2/ssDNA interaction were used, so this ATP sensor should have high stability in principle. To investigate the stability of the constructed ATP biosensor, a control ATP biosensor was prepared, in which the WS_2 nanosheets were dropped on the MCE modified Au electrode, and the aptamer for ATP was dropped on the WS_2 surface. These two kinds of sensor were kept at 4 °C for 30 days. The ΔR_{ct} of the two sensors for one concentration of ATP (50 μM) was measured in five-day interval. As shown in Fig. 6, during 20 days, nearly no decrease has been observed in the ΔR_{ct} value for the constructed sensor for 50 μM ATP, and after 30 days there is only 4.2% decrease in the ΔR_{ct} value. For the control sensor, there is 45% decrease in the ΔR_{ct} value for the same concentration of ATP after 20 days, and only 25% of the ΔR_{ct} value is remained after 30 days. This result substantially indicates that constructed ATP sensor has high stability as expected, which may be due to the unique interaction between WS_2 and ssDNA.

To investigate the applicability of the aptasensor under realistic conditions, the human blood plasma samples were prepared. The plasma samples were pretreated according to the previously reported procedure [50]. Briefly, they were deproteinized by trichloroacetic acid and diluted with 25 mM Tris-HCl buffer (1:9). Subsequently, the different concentrations of ATP were spiked into the pretreated plasma and the concentrations of ATP in the as-prepared samples were assayed using the developed ATP aptasensor. Table S1 shows that the ATP aptasensor can be applied for the detection of ATP even in the complicated matrix under realistic conditions.

3.4. Electrochemical detection of Hg^{2+}

Hg^{2+} is a highly toxic heavy metal known for its severe effects on human health and the environment [51,52]. For testifying the generality of the integrated sensing platform, we fabricated a sensing strategy for Hg^{2+} using a mercury-specific oligonucleotide (MSO) probe, which can strongly and selectively bind Hg^{2+} due to the T–Hg^{2+}–T coordination. As shown in the scheme, instead of the ABA, the MSO probe was immobilized on WS_2/SH-DNA/Au electrode through the strong interaction between MSO and WS_2 nanosheet. MSO/WS_2/SH-DNA/Au electrode was immersed in different concentrations of Hg^{2+} and reacted for 1 h, and then EIS spectra were recorded. The R_{ct} value is nearly unchanged when the MSO/WS_2/SH-DNA/Au electrode (Fig. 7A, curve a) was immersed in the blank buffer for 1 h (Fig. 7A, curve b). However, when the MSO/WS_2/SH-DNA/Au electrode was reacted with 100 nM Hg^{2+}, a decrease in the R_{ct} value is obtained because MSO reacted with Hg^{2+} to form stable DNA duplexes, which can be easily dissociated from the WS_2 surface (Fig. 7A, curve c).

Fig. 7B shows the relationship between ΔR_{ct} and different Hg^{2+} concentrations in logarithmic scale. The ΔR_{ct} possesses a linear correlation to the logarithm of Hg^{2+} concentration in the range from 0.1 nM to 500 nM (R^2=0.991). The detection limit is about 0.5 pM (3σ), which is better than some previously reported electrochemical Hg^{2+} sensors [53,54]. To test the specificity of Hg^{2+} sensor, the interferences of other metal ions for detecting Hg^{2+} were performed, including Ca^{2+}, Cu^{2+}, Fe^{3+}, Mg^{2+}, Pb^{2+}, Ba^{2+}, Ag^{+}, Zn^{2+}(Fig. 7C). Compared with that of 100 nM Hg^{2+}, the response from these metal ions is less than 5%. So the interference of these relevant metal ions to this Hg^{2+} sensor is negligible. The Hg^{2+} sensor also showed high stability as that of the constructed ATP sensor.

4. Conclusion

In summary, for the first time, we reported that the unique WS_2-ssDNA interaction can be used to construct electrochemical aptasensors for ATP and Hg^{2+}. These two sensors showed high sensitivity, selectivity and stability due to the unique WS_2-ssDNA interactions and the specific aptamer-target recognition. It would be easy to generalize this strategy to detect a spectrum of targets using WS_2 and different aptamers. In addition, this sensing strategy can also be expanded to other analogous of WS_2, such as GO and MoS_2, which have been reported to possess the similar interactions with ssDNA as that of WS_2.

Conflict of interest

The author declares no competing financial interest.

Acknowledgement

The authors are thankful for the fundings from the National Natural Science Foundation of China (Grant no. 51402063), the Fundamental Research Funds of Shandong University (2014QY003), the “100 Talents Program” of the Chinese Academy of Sciences, and Scientific and Technological Innovation Team of Beijing Academy of Agricultural and Forestry Sciences (JNKYT201604).

Appendix A. Supporting information

Supplementary data associated with this article can be found in the online version at doi:10.1016/j.talanta.2016.10.088.

References

[1] Z.J. Guo, J.T. Ren, J.H. Wang, E.K. Wang, Single-walled carbon nanotubes based quenching of free FAM-aptamer for selective determination of ochratoxin A, Talanta 85 (2011) 2517–2521.

[2] K.C. Zhang, M. Liu, X.Y. Tong, N. Sun, L. Zhou, Y. Cao, J.E. Wang, H.L. Zhang, R.J. Pei, Aptamer-modified temperature-sensitive liposomal contrast agent for magnetic resonance imaging, Biomacromolecules 16 (2015) 2618–2623.
[3] L. Wang, M. Xu, L. Han, M. Zhou, C. Zhu, S. Dong, Graphene enhanced electron transfer at aptamer modified electrode and its application in biosensing, Anal. Chem. 84 (2012) 7301–7307.
[4] Y.R. Wu, K. Sefah, H.P. Liu, R.W. Wang, W.H. Tan, DNA aptamer-micelle as an efficient detection/delivery vehicle toward cancer cells, Proc. Natl. Acad. Sci. 107 (2010) 5–10.
[5] T.G. Cha, B.A. Baker, M.D. Sauffer, J. Salgado, D. Jaroch, J.J. Rickus, D.M. Porterfield, J.H. Choi, Optical nanosensor architecture for cell-signaling molecules using DNA aptamer-coated carbon nanotubes, ACS Nano 5 (2011) 4236–4244.
[6] W.H. Tan, M.J. Donovan, J.H. Jiang, Aptamers from cell-based selection for bioanalytical applications, Chem. Rev. 113 (2013) 2842–2862.
[7] J. Ge, E. Ou, R. Yu, X. Chu, A novel aptameric nanobiosensor based on the self-assembled DNA-MoS_2 nanosheet architecture for biomolecule detection, J. Mater. Chem. B 2 (2014) 625–628.
[8] C.Y. Zhang, L.W. Johnson, Single quantum-dot-based aptameric nanosensor for cocaine, Anal. Chem. 81 (2009) 3051–3055.
[9] S.J. Zhen, L.Q. Chen, S.J. Xiao, Y.F. Li, P.P. Hu, L. Zhan, L. Peng, E.Q. Song, C.Z. Huang, Carbon nanotubes as a low background signal platform for a molecular aptamer beacon on the basis of long-range resonance energy transfer, Anal. Chem. 82 (2010) 8432–8437.
[10] J. Zhang, L.H. Wang, H. Zhang, F. Boey, S.P. Song, C.H. Fan, Aptamer-based multicolor fluorescent gold nanoprobes for multiplex detection in homogeneous solution, Small 6 (2010) 201–204.
[11] H. Beitollahi, F. Ebadinejad, F. Shojaie, M. Torkzadeh-Mahani, A magnetic core–shell Fe_3O_4@SiO_2/MWCNT nanocomposite modified carbon paste electrode for amplified electrochemical sensing of amlodipine and hydrochlorothiazide, Anal. Methods 8 (2016) 6185–6193.
[12] H. Beitollahi, H. Karimi-Maleh, H. Khabazzadeh, Nanomolar and selective determination of epinephrine in the presence of norepinephrine using carbon paste electrode modified with carbon nanotubes and novel 2-(4-oxo-3-phenyl-3,4-dihydro-quinazolinyl)-N′-phenyl-hydrazinecarbothioamide, Anal. Chem. 80 (2008) 9848–9851.
[13] H. Beitollahi, A. Gholami, M.R. Ganjali, Preparation, characterization and electrochemical application of Ag–ZnO nanoplates for voltammetric determination of glutathione and tryptophan using modified carbon paste electrode, Mater. Sci. Eng.: C 57 (2015) 107–112.
[14] H. Beitollahi, S. Nekooei, Application of a modified CuO nanoparticles carbon paste electrode for simultaneous determination of isoperenaline, acetaminophen and N-acetyl-L-cysteine, Electroanalysis 28 (2016) 645–653.
[15] H. Beitollahi, S.G. Ivari, M. Torkzadeh-Mahani, Voltammetric determination of 6-thioguanine and folic acid using a carbon paste electrode modified with ZnO-CuO nanoplates and modifier, Mater. Sci. Eng.: C 69 (2016) 128–133.
[16] J.A. Mann, J. Rodriguez-Lopez, H.D. Abruna, W.R. Dichtel, Multivalent binding motifs for the noncovalent functionalization of graphene, J. Am. Chem. Soc. 133 (2011) 17614–17617.
[17] M. McMullan, N. Sun, P. Papakonstantinou, M. Li, W. Zhou, D. Mihailovic, Aptamer conjugated Mo(6)S(9–x)I(x) nanowires for direct and highly sensitive electrochemical sensing of thrombin, Biosens. Bioelectron. 26 (2011) 1853–1859.
[18] F. Li, J.J. Li, C. Wang, J. Zhang, X.F. Li, X.C. Le, Competitive protection of aptamer-functionalized gold nanoparticles by controlling the DNA assembly, Anal. Chem. 83 (2011) 6464–6467.
[19] S.Q. Yu, G.Z. Zou, Q. Wei, Ultrasensitive electrochemical immunosensor for quantitative detection of tumor specific growth factor by using Ag@CeO_2 nanocomposite as labels, Talanta 156 (2016) 11–17.
[20] M. Xu, T. Liang, M. Shi, H. Chen, Graphene-Like two-dimensional materials, Chem. Rev. 113 (2013) 3766–3798.
[21] X. Huang, Z. Zeng, H. Zhang, Metal dichalcogenide nanosheets: preparation, properties and applications, Chem. Soc. Rev. 42 (2013) 1934–1946.
[22] S.Z. Butler, S.M. Hollen, L. Cao, Y. Cui, J.A. Gupta, H.R. Gutiérrez, T.F. Heinz, S.S. Hong, J. Huang, A.F. Ismach, E.J. Halperin, M. Kuno, V.V. Plashnitsa, R.D. Robinson, R.S. Ruoff, S. Salahuddin, J. Shan, L. Shi, M.G. Spencer, M. Terrones, W. Windl, J.E. Berger, Progress, challenges, and opportunities in two-dimensional materials beyond graphene, ACS Nano 7 (2013) 2898–2926.
[23] M. Chhowalla, H.S. Shin, G. Eda, L.J. Li, K.P. Loh, H. Zhang, The chemistry of two-dimensional layered transition metal dichalcogenide nanosheets, Nat. Chem. 5 (2013) 263–275.
[24] W. Li, R. Zamani, M. Ibanez, D. Cadavid, A. Shavel, J.R. Morante, J. Arbiol, A. Cabot, Metal ions to control the morphology of semiconductor nanoparticles: copper selenide nanocubes, J. Am. Chem. Soc. 135 (2013) 4664–4667.
[25] M. Vasei, P. Das, H. Cherfouth, B. Marsan, J.P. Claverie, TiO_2@C core-shell nanoparticles formed by polymeric nano-encapsulation, Front. Chem. (2014). http://dx.doi.org/10.3389/fchem.2014.00047.
[26] H. Huang, T. Chen, X. Liu, H. Ma, Ultrasensitive and simultaneous detection of heavy metal ions based on three-dimensional graphene-carbon nanotubes hybrid electrode materials, Anal. Chim. Acta 852 (2014) 45–54.
[27] X. Ma, T. Miao, W. Zhu, X. Gao, C. Wang, C. Zhao, H. Ma, Electrochemical detection of nitrite based on glassy carbon electrode modified with gold-polyaniline-graphene nanocomposites, RSC Adv. 4 (2014) 57842–57849.
[28] W.J. Zhao, Z. Ghorannevis, L.Q. Chu, M.L. Toh, C. Kloc, P.H. Tan, G. Eda, Evolution of electronic structure in atomically thin sheets of WS_2 and WSe_2, ACS Nano 7 (2013) 791–797.
[29] M. Bernardi, M. Palummo, J.C. Grossman, Extraordinary sunlight absorption and one nanometer thick photovoltaics using two-dimensional monolayer materials, Nano Lett. 13 (2013) 3664–3670.
[30] X. Liu, J. Ge, X. Wang, Z. Wu, G. Shen, R. Yu, Development of a highly sensitive sensing platform for T4 polynucleotide kinase phosphatase and its inhibitors based on WS_2 nanosheets, Anal. Methods 6 (2014) 7212–7217.
[31] A. Gasnier, M.L. Pedano, M.D. Rubianes, G.A. Rivas, Graphene paste electrode: electrochemical behavior and analytical applications for the quantification of NADH, Sens. Actuators B Chem. 176 (2013) 921–926.
[32] X. Wang, H. Zhu, Y. Bao, F. Yang, X. Yang, Uniform hierarchical frameworks patterned by movable magnetic microparticles, ACS Nano 5 (2011) 3250–3256.
[33] C. Wang, H. Luo, Z. Zhang, Y. Wu, J. Zhang, S. Chen, Removal of As(III) and As(V) from aqueous solutions using nanoscale zero valent iron-reduced graphite oxide modified composites, J. Hazard. Mater. 268 (2014) 124–131.
[34] N. Li, A. Than, X. Wang, S.H. Xu, L. Sun, P. Chen, Profiling metabolites using functionalized graphene quantum dots, ACS Nano 10 (2016) 3622–3629.
[35] S.J. He, B. Song, D. Li, C.F. Zhu, W.P. Qi, Y.Q. Wen, L.H. Wang, S.P. Song, H.P. Fang, C.H. Fan, A graphene nanoprobe for rapid, sensitive, and multicolor fluorescent DNA analysis, Adv. Funct. Mater. 20 (2010) 453–459.
[36] Y. Dong, M. Liu, Y. Liu, S. Wang, J. Li, Molybdenum-doped mesoporous carbon/graphene composites as efficient electrocatalysts for the oxygen reduction, J. Mater. Chem. A 3 (2015) 19969–19973.
[37] S.K. Cushing, M. Li, F. Huang, N. Wu, Origin of strong excitation wavelength dependent fluorescence of graphene oxide, ACS Nano 8 (2014) 1002–1013.
[38] F.K. Meng, J. Li, S.K. Cushing, M. Zhi, N.Q. Wu, Solar hydrogen generation by nanoscale p-n junction of p-type molybdenum disulfide/n-type nitrogen-doped reduced graphene oxide, J. Am. Chem. Soc. 135 (2013) 10286–10289.
[39] C. Zhu, Z. Zeng, H. Li, F. Li, C. Fan, H. Zhang, Single-layer MoS_2-based nanoprobes for homogeneous detection of biomolecules, J. Am. Chem. Soc. 135 (2013) 5998–6001.
[40] Q. Xi, D.M. Zhou, Y.Y. Kan, J. Ge, Z.K. Wu, R.Q. Yu, J.H. Jiang, Highly sensitive and selective strategy for MicroRNA detection based on WS_2 nanosheet mediated fluorescence quenching and duplex-specific nuclease signal amplification, Anal. Chem. 86 (2014) 1361–1365.
[41] Y. Yuan, R. Li, Z. Liu, Establishing water-soluble layered WS_2 nanosheet as a platform for biosensing, Anal. Chem. 86 (2014) 3610–3615.
[42] S. Wang, Y. Zhang, Y. Ning, G.J. Zhang, A WS_2 nanosheet-based platform for fluorescent DNA detection via PNA–DNA hybridization, Analyst 140 (2015) 434–439.
[43] S. Ratha, C.S. Rout, Supercapacitor electrodes based on layered tungsten disulfide reduced graphene oxide hybrids synthesized by a facile hydrothermal method, ACS Appl. Mater. Interfaces 5 (2013) 11427–11433.
[44] K.J. Huang, Y.J. Liu, J.Z. Zhang, Y.M. Liu, A novel aptamer sensor based on layered tungsten disulfide nanosheets and Au nanoparticles amplification for 17b-estradiol detection, Anal. Methods 6 (2014) 8011–8017.
[45] X. Xie, K. Zhao, X. Xu, W. Zhao, S. Liu, Z. Zhu, M. Li, Z. Shi, Y. Shao, Study of heterogeneous electron transfer on the graphene/self-assembled monolayer modified gold electrode by electrochemical approaches, J. Phys. Chem. C 114 (2010) 14243–14250.
[46] Z. Wang, J. Zhang, P. Chen, X. Zhou, Y. Yang, S. Wu, L. Niu, Y. Han, L. Wang, P. Chen, F. Boey, Q. Zhang, B. Liedberg, H. Zhang, Label-free, electrochemical detection of methicillin-resistant Staphylococcus aureus DNA with reduced graphene oxide-modified electrodes, Biosens. Bioelectron. 26 (2011) 3881–3886.
[47] A. Bonanni, M. Pumera, Graphene platform for hairpin-DNA based impedimetric genosensing, ACS Nano 5 (2011) 2356–2361.
[48] J. Yoshizumi, S. Kumamoto, M. Nakamura, K. Yamana, Target-induced strand release (TISR) from aptamer-DNA duplex: a general strategy for electronic detection of biomolecules ranging from a small molecule to a large protein, Analyst 133 (2008) 323–325.
[49] M. Zayats, Y. Huang, R. Gill, C.A. Ma, I. Willner, Label-free and reagentless aptamer-based sensors for small molecules, J. Am. Chem. Soc. 128 (2006) 13666–13667.
[50] J.M. Berg, J.L. Tymoczko, L. Stryer, Biochemistry, 5th ed., W.H. Freeman, New York, 2002.
[51] S. Cosnier, C. Mousty, A. Guelorget, M. Sanchez, A fast and direct amperometric determination of Hg^{2+} by a bienzyme electrode based on the competitive activities of glucose oxidase and laccase, Electroanalysis 23 (2011) 1776–1779.
[52] H. Park, S. Hwang, K. Kim, An electrochemical detection of Hg^{2+} ion using graphene oxide as an electrochemically active indicator, Electrochem. Commun. 24 (2012) 100–103.
[53] Y. Liao, Q. Li, N. Wang, S. Shao, Development of a new electrochemical sensor for determination of Hg(II) based on bis(indolyl)methane/mesoporous carbon nanofiber/Nafion/glassy carbon electrode, Sens. Actuators B 215 (2015) 592–597.
[54] Y. Yang, M. Kang, S. Fang, M. Wang, L. He, J. Zhao, H. Zhang, Z. Zhang, Electrochemical biosensor based on three-dimensional reduced graphene oxide and polyaniline nanocomposite for selective detection of mercury ions, Sens. Actuators B 214 (2015) 63–69.